Supporting Information

K^+ Modulated K^+/Vacancy Disordered Layered Oxide for High-Rate and High-Capacity Potassium-Ion Batteries

Zhitong Xiao,[a,†] Jiashen Meng,[a,†] Fanjie Xia,[a,b] Jinsong Wu,*[a,b] Fang Liu,[a,b] Xiao Zhang,[a] Linhan Xu,[c] Xinming Lin[a] and Liqiang Mai*[a,d]

[a]State Key Laboratory of Advanced Technology for Materials Synthesis and Processing, School of Materials Science and Engineering, Wuhan University of Technology, Luoshi Road 122, Wuhan, 430070, P. R. China.

[b]Nanostructure Research Centre (NRC), Wuhan University of Technology, Luoshi Road 122, Wuhan, 430070, P. R. China.

[c]Department of Physics, Collaborative Innovation Center for Optoelectronic Semiconductors and Efficient Devices, Jiujiang Research Institute, Xiamen University, Xiamen, 361005, P. R. China.

[d]Foshan Xianhu Laboratory of the Advanced Energy Science and Technology Guangdong Laboratory, Xianhu Hydrogen Valley, Foshan, 528200, P. R. China.

[†]These authors contributed equally: Zhitong Xiao and Jiashen Meng.

*Correspondence to: wujs@whut.edu.cn; mlq518@whut.edu.cn

Experimental Section

Materials synthesis

All reactants are analytical grade. In a typical synthesis for $K_xMn_{0.7}Ni_{0.3}O_2$, 4 g polyvinylpyrrolidone (PVP K90, M_w= 1 300 000) was added in 40 mL deionized water and stirred vigorously for 2 h. Then, a certain amount of KNO_3 (1.05, 1.575, 2.1, 2.625, 3.15, 3.675, 4.2, and 4.725 mmol for $K_{0.2}Mn_{0.7}Ni_{0.3}O_2$, $K_{0.3}Mn_{0.7}Ni_{0.3}O_2$, $K_{0.4}Mn_{0.7}Ni_{0.3}O_2$, $K_{0.5}Mn_{0.7}Ni_{0.3}O_2$, $K_{0.6}Mn_{0.7}Ni_{0.3}O_2$, $K_{0.7}Mn_{0.7}Ni_{0.3}O_2$, $K_{0.8}Mn_{0.7}Ni_{0.3}O_2$ and $K_{0.9}Mn_{0.7}Ni_{0.3}O_2$, respectively; all K 5% excess), 3.5 mmol $Mn(CH_3COO)_2{\cdot}4H_2O$ and 1.5 mmol $Ni(CH_3COO)_2{\cdot}4H_2O$ were dissolved in the obtained solution and stirred continuously for 8 h at room temperature. The mixed solution was dried at 70 °C for 12 h and pre-sintered at 300 °C for 2 h in air to obtain a black solid. Finally, the black solid was calcined at 900 °C for 10 h in air to obtain $K_xMn_{0.7}Ni_{0.3}O_2$ (x = 0.2, 0.3, 0.4, 0.5, 0.6, 0.7, 0.8, and 0.9). Due to the instability of these materials under ambient atmosphere, the products were collected at 100 °C and transferred promptly to an Ar atmosphere filled glove box. The soft carbon was synthesized by pyrolysis of 3,4,9,10-perylenetetracarboxylic dianhydride (PTCDA) at 900 °C for 10 h under flowing Ar atmosphere.[1]

Characterizations

XRD measurement was measured by a D8 Discover X-ray diffractometer with the non-monochromated Cu Kα X-ray as the source (λ = 1.5406 Å). TOPAS 4.2 software was used to perform XRD Rietveld refinement. SEM measurement was measured by a JEOL JSM-7100F with 20 kV acceleration voltage. ICP measurement was recorded with a PerkinElmer Optima 4300DV spectrometer. TEM, HAADF-STEM, HRTEM images, and SAED patterns were collected with a JEM-2100F and a Thermo Fischer Titan G2 60-300 microscope. The elemental mapping was conducted by an EDX-GENESIS 60S spectrometer. The STEM characterization was performed on a Thermo Fischer Titan Themis STEM with 300 kV acceleration voltage. The STEM images were obtained by an ABF detector and a HAADF detector, respectively. XPS test was

performed by a VG MultiLab 2000 instrument. For the sample preparation, the $K_{0.4}Mn_{0.7}Ni_{0.3}O_2$ and $K_{0.7}Mn_{0.7}Ni_{0.3}O_2$ cathode coin cells were charged to 3.9 V or charged to 3.9 V and then discharged to 2.0 V (*vs* K^+/K) at 20 mA g^{-1}. After the end of charging or discharging process, the coin cells were disassembled rapidly, and be careful not to short-circuit. The electrode products were harvested *via* washed with diethyl carbonate (DEC) and ethanol, before being dried at room temperature in Ar atmosphere filled glove box. For the *in situ* XRD measurement, $K_{0.4}Mn_{0.7}Ni_{0.3}O_2$ and $K_{0.7}Mn_{0.7}Ni_{0.3}O_2$ cathode *in situ* batteries were charged to 3.9 V and then discharged to 2.0 V (*vs* K^+/K) at 0.05 A g^{-1}, with 2θ within range from 24° to 28° and 35° to 43.5°.

Electrochemical measurements

The electrochemical tests were measured by using CR2016 coin cells, which used a potassium metal foil as counter electrode, a Grade GF/D Whatman glass microfiber filter as separator and a 0.8 M potassium hexafluorophosphate (KPF_6) in ethylene carbon (EC)- DEC with 1 : 1 volume ratio as electrolyte. The cathode was composed of 70 wt% $K_xMn_{0.7}Ni_{0.3}O_2$ (x = 0.2, 0.3, 0.4, 0.5, 0.6, 0.7, 0.8, and 0.9), 10 wt% polyvinylidene fluoride (PVDF) and 20 wt% acetylene black and coated onto Al foil. The anode was composed of 70 wt% soft carbon, 20 wt% acetylene black and 10 wt% carboxymethyl cellulose (CMC) binder and coated onto Cu foil. The area loading of cathode and anode materials were approximately 2.7-3.8 mg cm^{-2} and 3.2-4.3 mg cm^{-2}, respectively. For high mass loading electrochemical measurements, the cathode was composed of 90 wt% $K_{0.7}Mn_{0.7}Ni_{0.3}O_2$, 5 wt% PVDF and 5 wt% acetylene black and coated onto Al foil. The area loading of cathode materials was approximately 10 mg cm^{-2}. Galvanostatic discharge/charge tests were obtained using a LAND CT2001A multichannel testing system. GITT curve was also measured using a LAND CT2001A multichannel testing system, which conducted at a pulse current of 20 mA g^{-1} for 5 min, followed with a relaxation for 30 min. EIS and CV measurements were conducted with an Auto lab PGSTAT 302N and CHI 600e electrochemical workstation.

Molecular dynamics simulation calculation

The K^+ transport properties in $K_{0.4}Mn_{0.7}Ni_{0.3}O_2$ and $K_{0.7}Mn_{0.7}Ni_{0.3}O_2$ were investigated *via* molecular dynamics simulation method.[2] When carried out the molecular dynamic simulation calculations at 500 K, the Nose-Hoover thermostat used a 1 fs time step to simulate a 10 ps total time. The ionic transport behaviors of the system can be simulated by mean square displacements (MSD)

$$MSD(t) = \langle |r_i(t) - r_i(0)|^2 \rangle$$

where $r_i(t)$ is the position of the i-th K^+ at the time t.

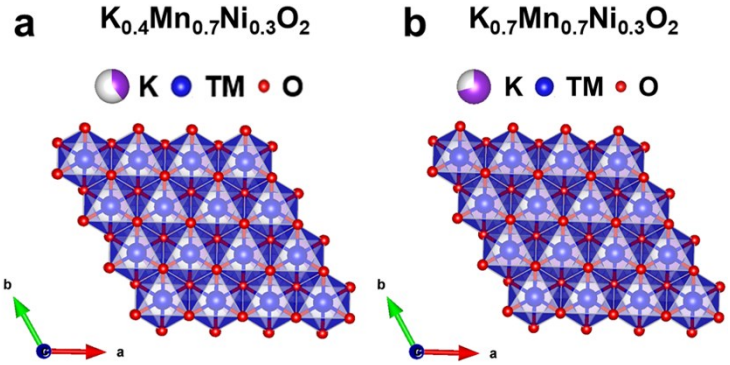

Fig. S1 Schematic illustration of $K_{0.4}Mn_{0.7}Ni_{0.3}O_2$ (a) and $K_{0.7}Mn_{0.7}Ni_{0.3}O_2$ (b) crystal viewed along the [001] zone axis.

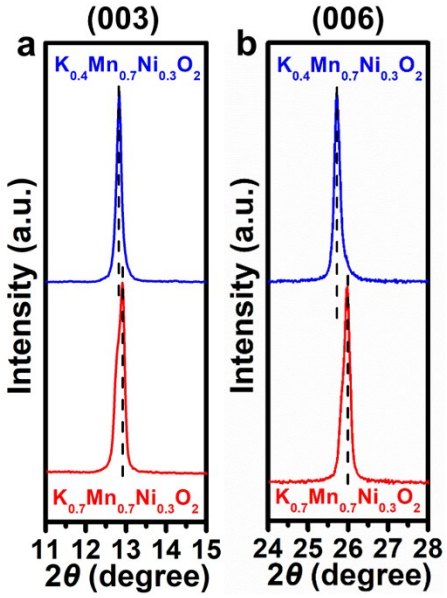

Fig. S2 Zoom-in images of XRD patterns of $K_{0.4}Mn_{0.7}Ni_{0.3}O_2$ and $K_{0.7}Mn_{0.7}Ni_{0.3}O_2$ for (003) peaks (a) and (006) peaks (b).

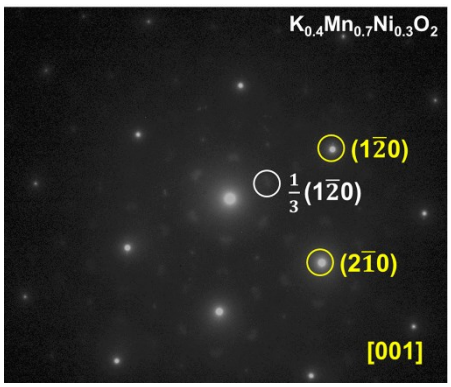

Fig. S3 SAED pattern of $K_{0.4}Mn_{0.7}Ni_{0.3}O_2$ along the [001] zone axis.

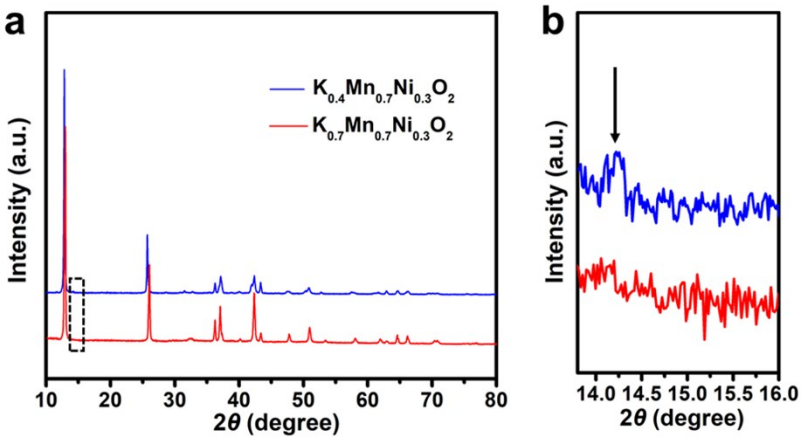

Fig. S4 (a) XRD patterns of $K_{0.4}Mn_{0.7}Ni_{0.3}O_2$ and $K_{0.7}Mn_{0.7}Ni_{0.3}O_2$. (b) Enlarged XRD patterns of $K_{0.4}Mn_{0.7}Ni_{0.3}O_2$ and $K_{0.7}Mn_{0.7}Ni_{0.3}O_2$ between 13.8° to 16.0°.

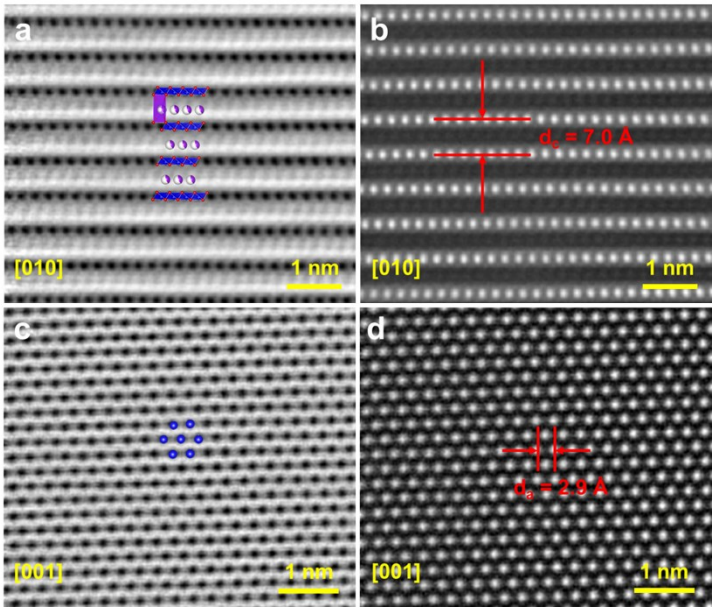

Fig. S5 ABF-STEM (a) and HAADF-STEM (b) images of $K_{0.4}Mn_{0.7}Ni_{0.3}O_2$ along the [010] zone axis. ABF-STEM (c) and HAADF-STEM (d) images of $K_{0.4}Mn_{0.7}Ni_{0.3}O_2$ along the [001] zone axis.

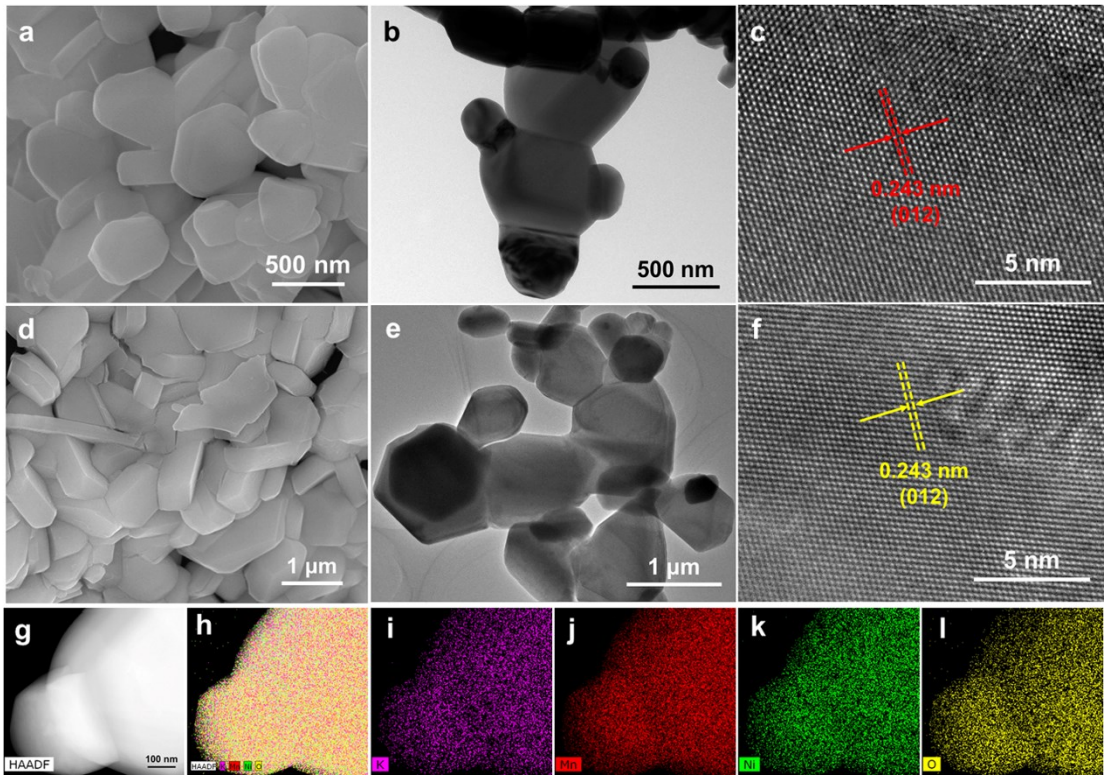

Fig. S6 SEM (a), TEM (b) and HRTEM (c) images of $K_{0.4}Mn_{0.7}Ni_{0.3}O_2$. SEM (d), TEM (e) and HRTEM (f) images of $K_{0.7}Mn_{0.7}Ni_{0.3}O_2$. (g-l) HAADF-STEM image of $K_{0.4}Mn_{0.7}Ni_{0.3}O_2$ and the corresponding EDS mappings for K, Mn, Ni, and O elements.

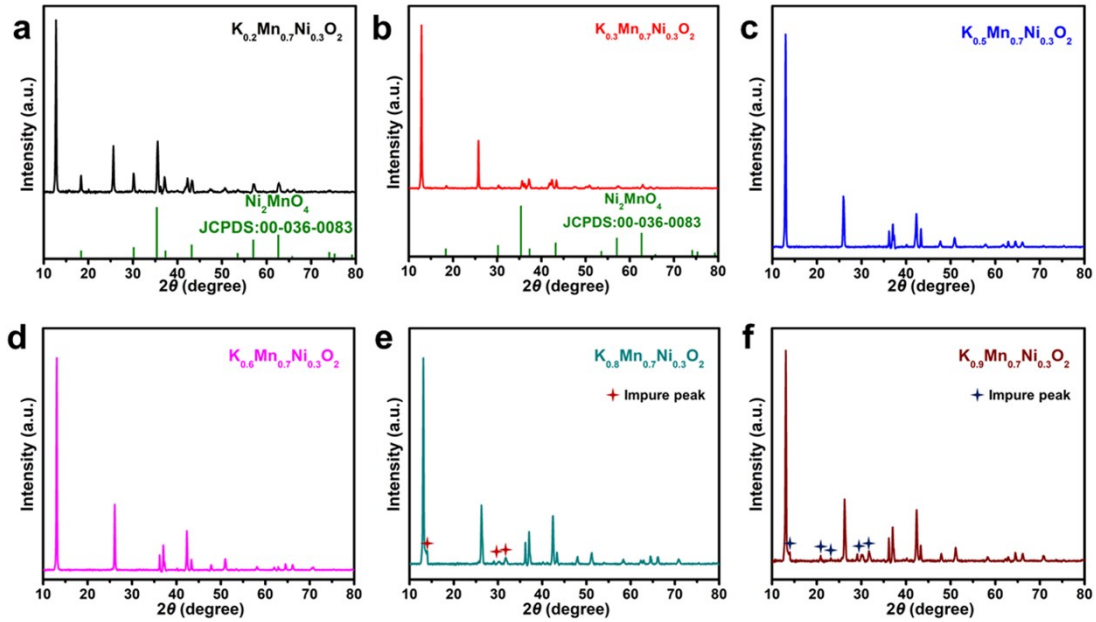

Fig. S7 XRD patterns of $K_{0.2}Mn_{0.7}Ni_{0.3}O_2$ (a), $K_{0.3}Mn_{0.7}Ni_{0.3}O_2$ (b), $K_{0.5}Mn_{0.7}Ni_{0.3}O_2$ (c), $K_{0.6}Mn_{0.7}Ni_{0.3}O_2$ (d), $K_{0.8}Mn_{0.7}Ni_{0.3}O_2$ (e), and $K_{0.9}Mn_{0.7}Ni_{0.3}O_2$ (f), respectively.

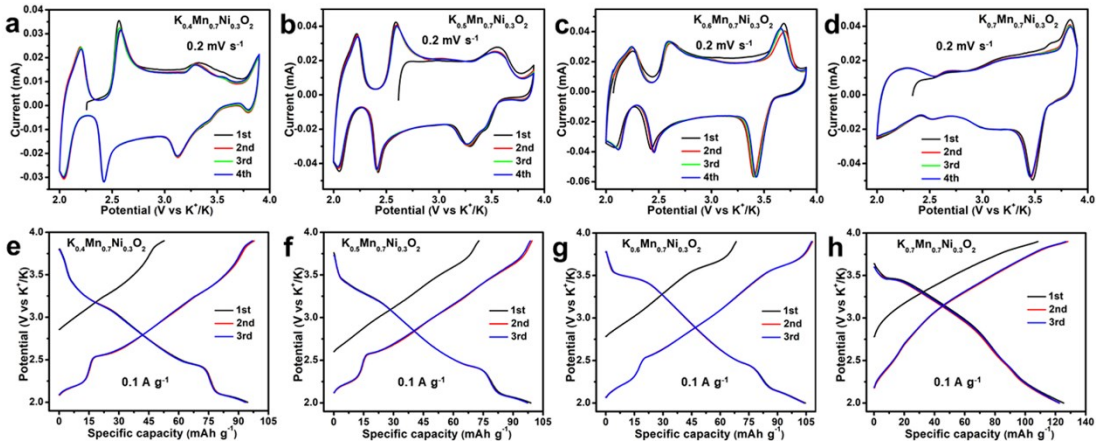

Fig. S8 (a-d) CV curves of the first four cycles at 0.2 mV s^{-1} of $K_{0.4}Mn_{0.7}Ni_{0.3}O_2$, $K_{0.5}Mn_{0.7}Ni_{0.3}O_2$, $K_{0.6}Mn_{0.7}Ni_{0.3}O_2$, and $K_{0.7}Mn_{0.7}Ni_{0.3}O_2$, respectively. (e-h) Charge/discharge curves (for the 1st, 2nd and 3rd cycle at 0.1 A g^{-1}) of $K_{0.4}Mn_{0.7}Ni_{0.3}O_2$, $K_{0.5}Mn_{0.7}Ni_{0.3}O_2$, $K_{0.6}Mn_{0.7}Ni_{0.3}O_2$, and $K_{0.7}Mn_{0.7}Ni_{0.3}O_2$, respectively.

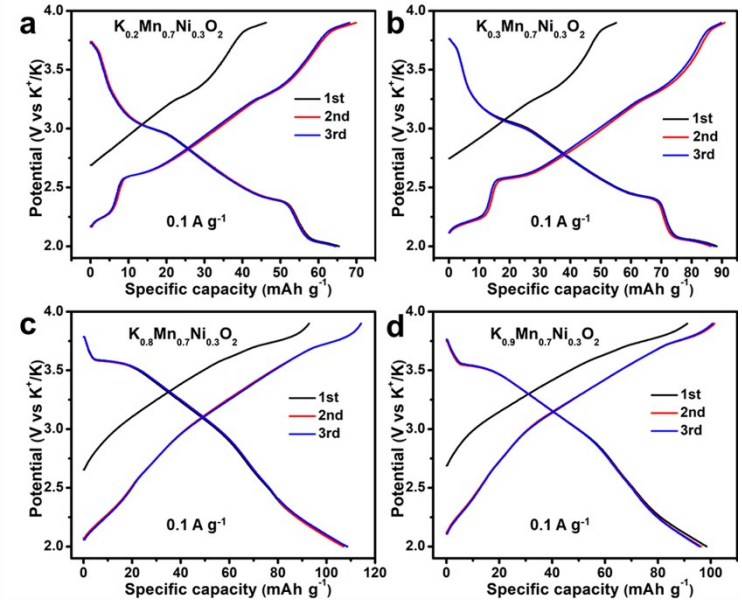

Fig. S9 (a-d) Charge/discharge curves (for the 1st, 2nd and 3rd cycle at 0.1 A g^{-1}) of $K_{0.2}Mn_{0.7}Ni_{0.3}O_2$, $K_{0.3}Mn_{0.7}Ni_{0.3}O_2$, $K_{0.8}Mn_{0.7}Ni_{0.3}O_2$, and $K_{0.9}Mn_{0.7}Ni_{0.3}O_2$, respectively.

Four pairs of voltage plateaus are observed in the charge/discharge curves of $K_{0.2}Mn_{0.7}Ni_{0.3}O_2$ and $K_{0.3}Mn_{0.7}Ni_{0.3}O_2$, which are similar to $K_{0.4}Mn_{0.7}Ni_{0.3}O_2$ (Fig. S9 a, b). The typical charge/discharge curves of $K_{0.8}Mn_{0.7}Ni_{0.3}O_2$ and $K_{0.9}Mn_{0.7}Ni_{0.3}O_2$

show sloping and smooth characteristic within a large range of voltage, which are similar to $K_{0.7}Mn_{0.7}Ni_{0.3}O_2$ (Fig. S9 c, d). However, due to the presence of impurities, their specific capacities (65 mA h g^{-1} for $K_{0.2}Mn_{0.7}Ni_{0.3}O_2$, 87 mA h g^{-1} for $K_{0.3}Mn_{0.7}Ni_{0.3}O_2$, 107 mA h g^{-1} for $K_{0.8}Mn_{0.7}Ni_{0.3}O_2$ and 95 mA h g^{-1} for $K_{0.9}Mn_{0.7}Ni_{0.3}O_2$) are lower than that of $K_{0.4}Mn_{0.7}Ni_{0.3}O_2$ (94 mA h g^{-1}) and $K_{0.7}Mn_{0.7}Ni_{0.3}O_2$ (124 mA h g^{-1}), respectively.

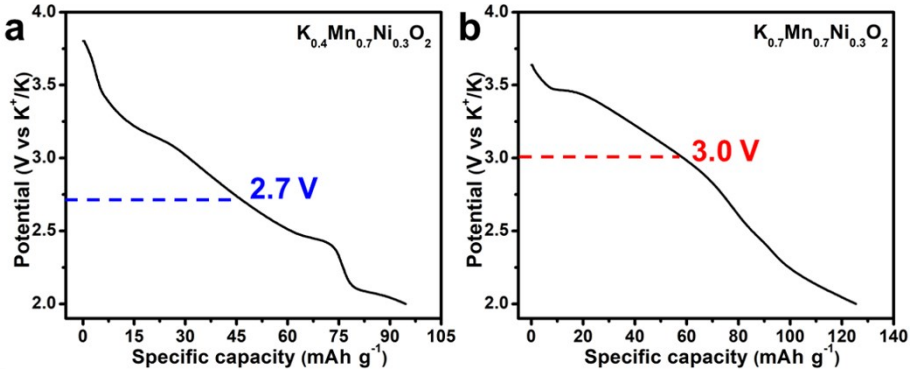

Fig. S10 Discharge curves for the 1st cycle at 0.1 A g^{-1} of $K_{0.4}Mn_{0.7}Ni_{0.3}O_2$ (a) and $K_{0.7}Mn_{0.7}Ni_{0.3}O_2$ (b).

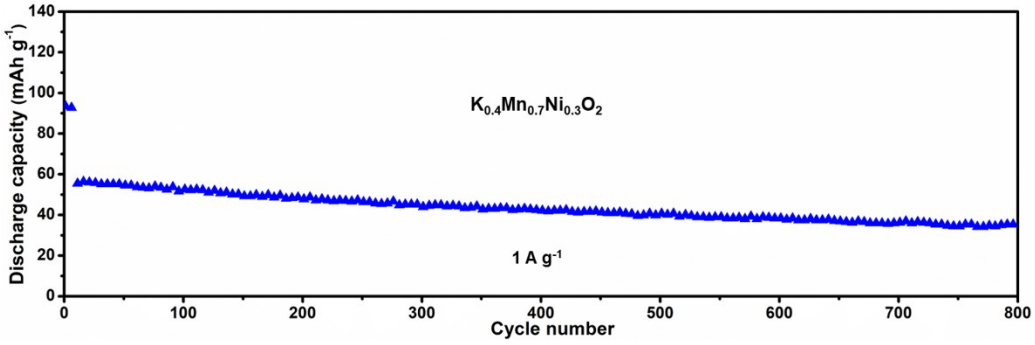

Fig. S11 Long-term cycling performance of $K_{0.7}Mn_{0.7}Ni_{0.3}O_2$ at 1 A g^{-1} (initial six cycles are tested at 0.1 A g^{-1} for activation of electrode material).

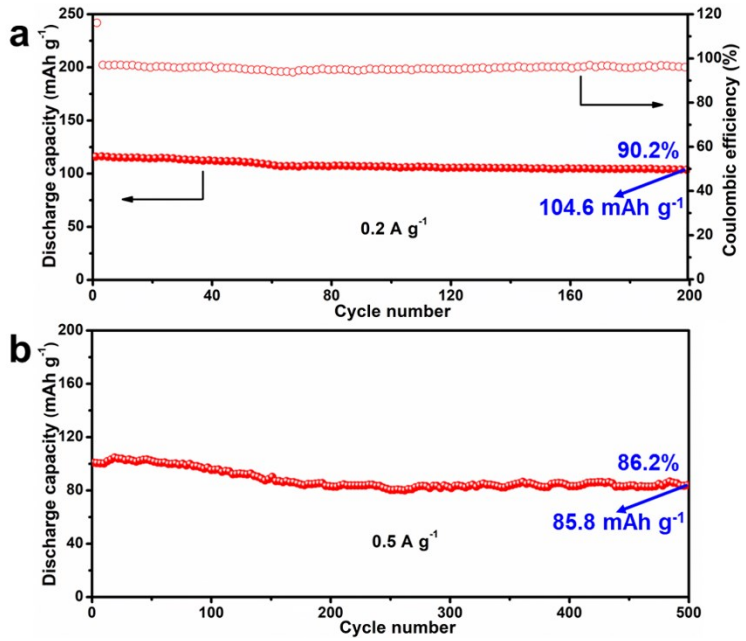

Fig. S12 (a) Cycling performance of $K_{0.7}Mn_{0.7}Ni_{0.3}O_2$ with Coulombic efficiencies measured at 0.2 A g^{-1}. (b) Long-term cycling performance of $K_{0.7}Mn_{0.7}Ni_{0.3}O_2$ at 0.5 A g^{-1}.

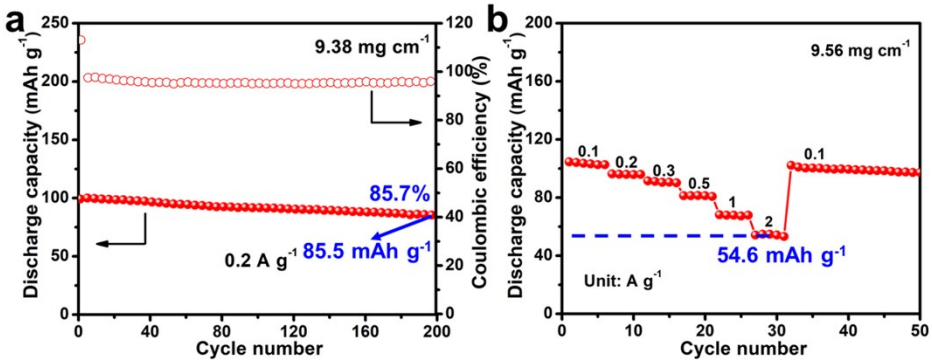

Fig. S13 Cycling and rate performances of $K_{0.7}Mn_{0.7}Ni_{0.3}O_2$ at the high mass loadings. (a) Cycling performance with Coulombic efficiencies measured at 0.2 A g^{-1}. (b) Rate performance conducted at 0.1, 0.2, 0.3, 0.5, 1, 2, and back to 0.1 A g^{-1}.

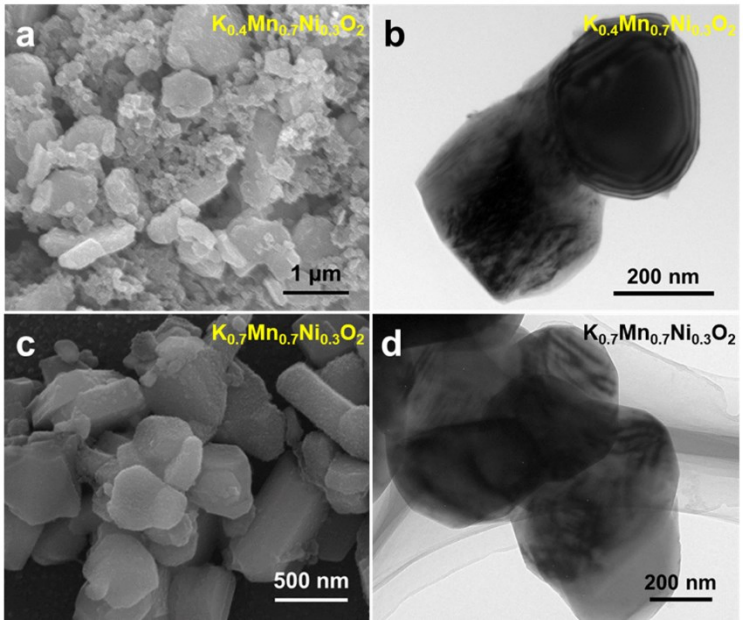

Fig. S14 (a, b) SEM and TEM images after 150 cycles at 0.1 A g^{-1} for $K_{0.4}Mn_{0.7}Ni_{0.3}O_2$. (c, d) SEM and TEM images after 150 cycles at 0.1 A g^{-1} for $K_{0.7}Mn_{0.7}Ni_{0.3}O_2$.

The particle morphologies of both $K_{0.4}Mn_{0.7}Ni_{0.3}O_2$ and $K_{0.7}Mn_{0.7}Ni_{0.3}O_2$ are well-preserved after cycling.

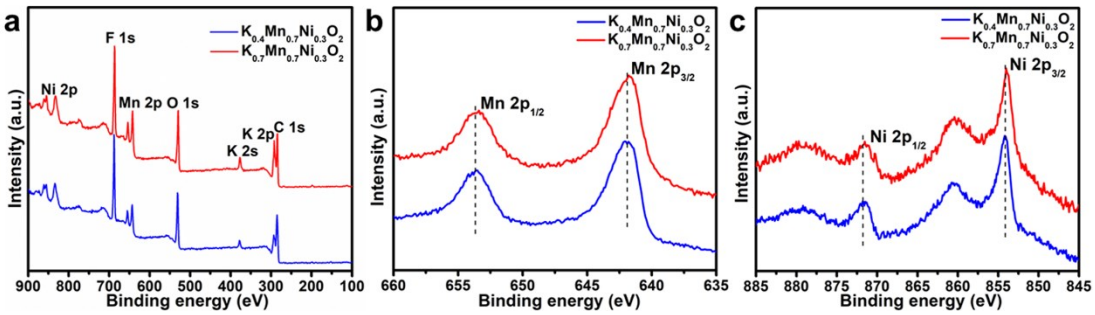

Fig. S15 XPS survey spectra (a) and the corresponding spectra of Mn 2p (b) and Ni 2p (c) for $K_{0.4}Mn_{0.7}Ni_{0.3}O_2$ and $K_{0.7}Mn_{0.7}Ni_{0.3}O_2$ electrodes before cycling.

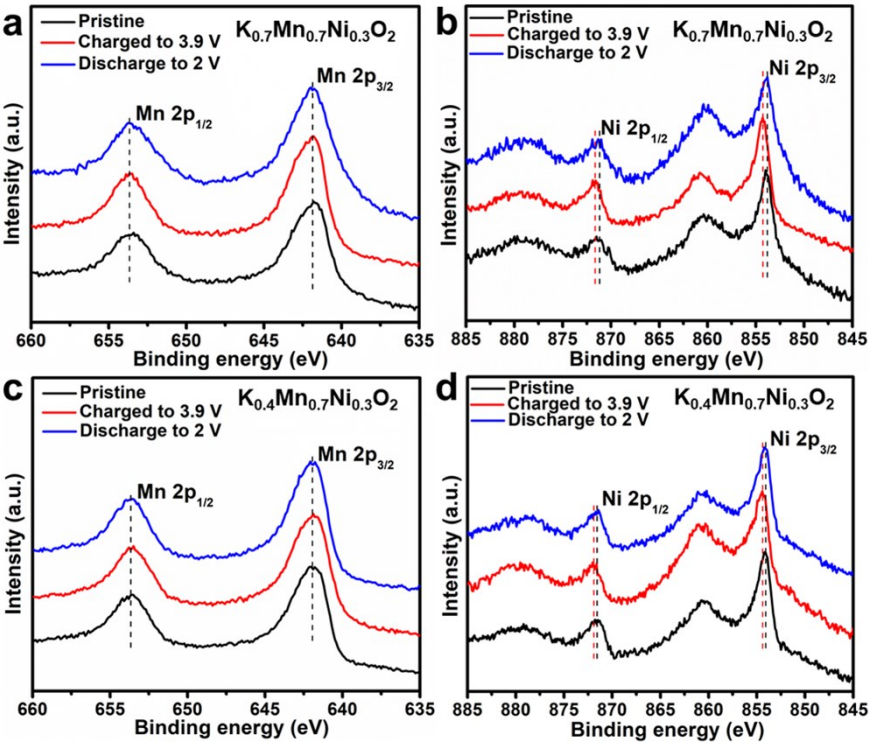

Fig. S16 XPS spectra of Mn 2p and Ni 2p for $K_{0.7}Mn_{0.7}Ni_{0.3}O_2$ (a, b) and $K_{0.4}Mn_{0.7}Ni_{0.3}O_2$ (c, d) at different charge/discharge states.

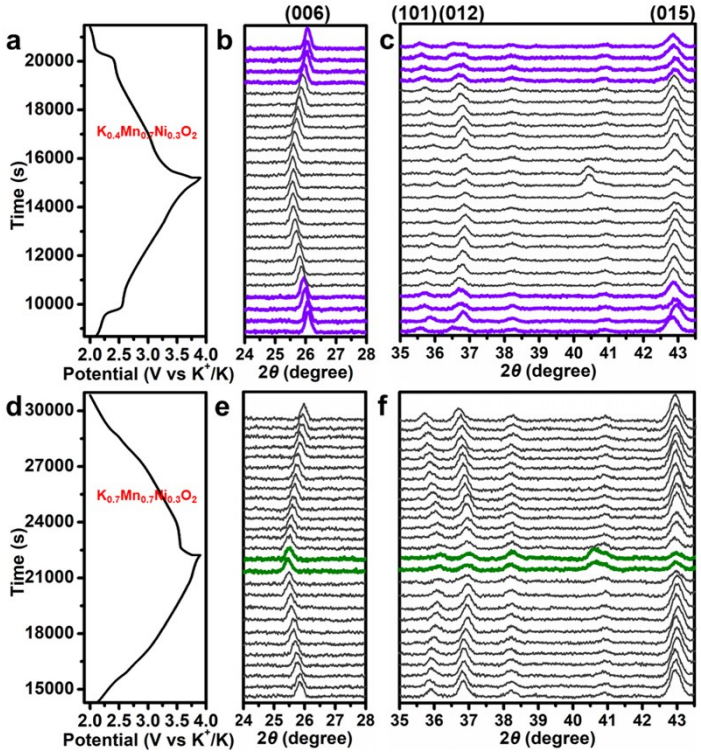

Fig. S17 One-dimensional *in situ* XRD patterns at 24-28° and 35-43.5° of $K_{0.4}Mn_{0.7}Ni_{0.3}O_2$ (a-c) and $K_{0.7}Mn_{0.7}Ni_{0.3}O_2$ (d-f) during the second cycle.

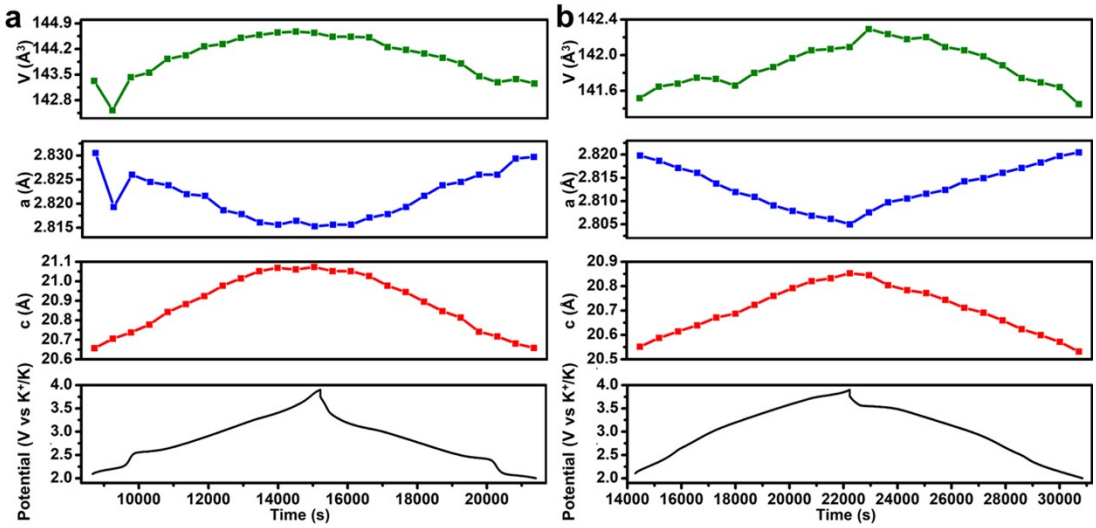

Fig. S18 The variation of lattice parameters along with K^+ extraction and insertion for $K_{0.4}Mn_{0.7}Ni_{0.3}O_2$ (a) and $K_{0.7}Mn_{0.7}Ni_{0.3}O_2$ (b), respectively. These values were estimated from electrochemical *in situ* XRD results as shown in Fig. S17.

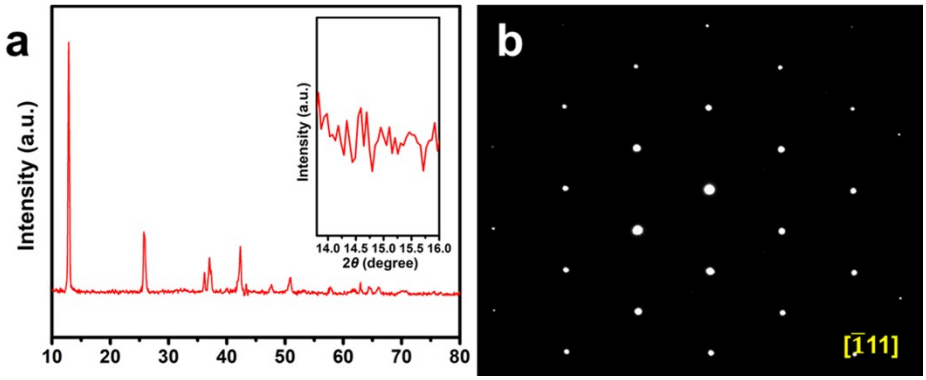

Fig. S19 XRD (a) and SAED (b) patterns of $K_{0.7}Mn_{0.7}Ni_{0.3}O_2$ when charged at 3.7 V (inset: enlarged XRD pattern between 13.8° to 16.0°).

When charged at 3.7 V with a low current density of 20 mA g^{-1}, the $K_{0.7}Mn_{0.7}Ni_{0.3}O_2$ electrode does not have the K^+/vacancy ordering peaks in the XRD pattern, and the K^+/vacancy ordered superlattice spots were not observed in the [-111] SAED pattern. It is indicated that the K^+/vacancy disordered structure remains during the charge and discharge process.

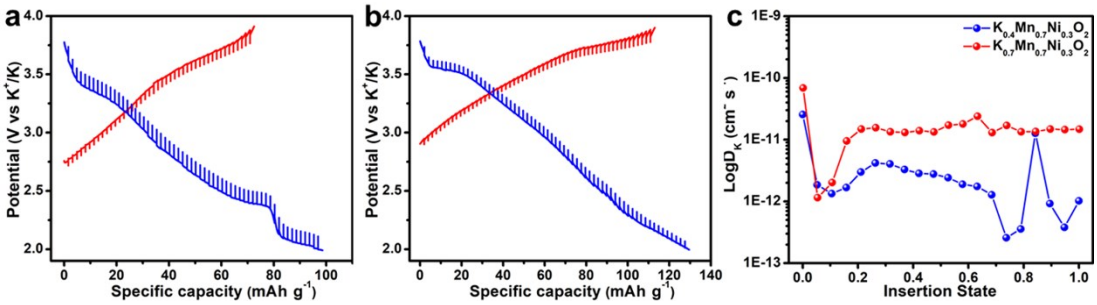

Fig. S20 GITT curves and chemical diffusion coefficients of $K_{0.4}Mn_{0.7}Ni_{0.3}O_2$ and $K_{0.7}Mn_{0.7}Ni_{0.3}O_2$. Potential response of $K_{0.4}Mn_{0.7}Ni_{0.3}O_2$ (a) and $K_{0.7}Mn_{0.7}Ni_{0.3}O_2$ (b) during GITT measurement. (c) The calculated chemical diffusion coefficient for K^+.

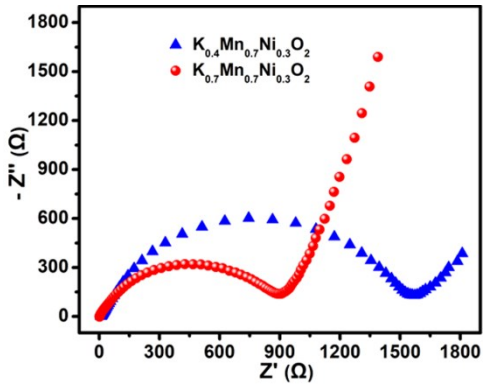

Fig. S21 Nyquist plots of $K_{0.4}Mn_{0.7}Ni_{0.3}O_2$ and $K_{0.7}Mn_{0.7}Ni_{0.3}O_2$.

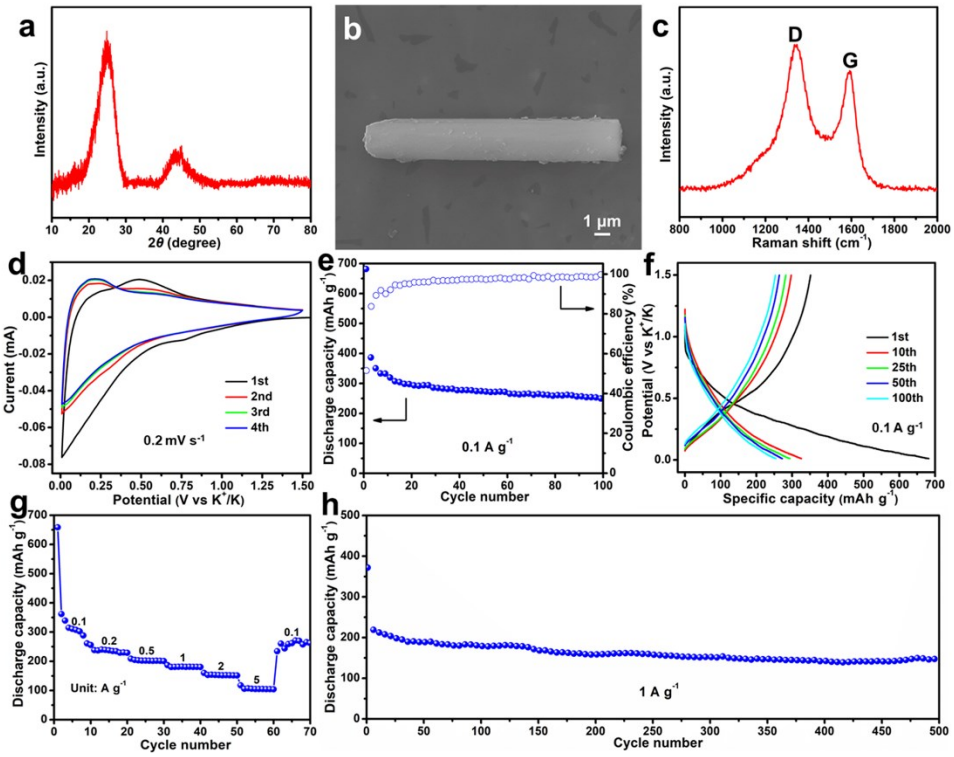

Fig. S22 Structural and morphology characterizations and electrochemical performances in the potential range of 0.01-1.5 V of soft carbon. (a) XRD pattern. (b) SEM image. (c) Raman spectrum. (d) CV curves of the first four cycles at 0.2 mV s^{-1}. (e) Cycling performance and the corresponding Coulombic efficiencies tested at 0.1 A g^{-1}. (f) Charge-discharge curves (for the 1st, 10th, 25th, 50th, and 100th cycle at 0.1 A g^{-1}). (g) Rate performance conducted at 0.1, 0.2, 0.5, 1, 2, 5, and back to 0.1 A g^{-1}. (h) Long-term cycling performance at 1 A g^{-1}.

Table S1. Structural parameters and atomic position of $K_{0.4}Mn_{0.7}Ni_{0.3}O_2$ from Rietveld refinement.

Formula		$K_{0.4}Mn_{0.7}Ni_{0.3}O_2$	
Crystal system		Hexagonal	
Space group		*R3m*	
Atom	*x*	*y*	*z*
K	0	0	0.8346
Mn	0	0	0
Ni	0	0	0
O	0	0	0.3792
O	0	0	0.6445
a = *b* (Å)		2.8858	
c (Å)		20.8494	
Cell volume ($Å^3$)		150.372	
Crystal density (g cm^{-3})		3.4852	
R_{wp} (%)		8.60	

Table S2. Structural parameters and atomic position of $K_{0.7}Mn_{0.7}Ni_{0.3}O_2$ from Rietveld refinement.

Formula		$K_{0.7}Mn_{0.7}Ni_{0.3}O_2$	
Crystal system		Hexagonal	
Space group		*R3m*	
Atom	*x*	*y*	*z*
K	0	0	0.8317
Mn	0	0	0
Ni	0	0	0
O	0	0	0.3817
O	0	0	0.6257
a = *b* (Å)		2.8879	
c (Å)		20.5893	
Cell volume (Å^3)		148.709	
Crystal density (g cm^{-3})		3.9171	
R_{wp} (%)		5.71	

Table S3. ICP measurement results of $K_xMn_{0.7}Ni_{0.3}O_2$ (x = 0.2, 0.3, 0.4, 0.5, 0.6, 0.7, 0.8, and 0.9).

Theoretical chemical formula	**K : Mn : Ni**
$K_{0.2}Mn_{0.7}Ni_{0.3}O_2$	0.219 : 0.700 : 0.305
$K_{0.3}Mn_{0.7}Ni_{0.3}O_2$	0.310 : 0.700 : 0.311
$K_{0.4}Mn_{0.7}Ni_{0.3}O_2$	0.398 : 0.700 : 0.304
$K_{0.5}Mn_{0.7}Ni_{0.3}O_2$	0.499 : 0.700 : 0.307
$K_{0.6}Mn_{0.7}Ni_{0.3}O_2$	0.596 : 0.700 : 0.304
$K_{0.7}Mn_{0.7}Ni_{0.3}O_2$	0.695 : 0.700 : 0.302
$K_{0.8}Mn_{0.7}Ni_{0.3}O_2$	0.783 : 0.700 : 0.309
$K_{0.9}Mn_{0.7}Ni_{0.3}O_2$	0.912 : 0.700 : 0.313

Table S4. Electrochemical performance comparison of various layered oxides cathode in PIBs.

Layered oxides cathode	Voltage range (V)	Current density (mA g^{-1})	Cycle number	Residual capacity (mAh g^{-1})	Capacity retention (%)	Average operating potential (V)	Specific energy (Wh kg^{-1})	Reference
P3-type $K_{0.7}Mn_{0.7}Ni_{0.3}O_2$	**2.0-3.9**	**100** **1000**	**100** **800**	**117.4** **78.8**	**93.6** **88.5**	**3.0**	**390**	**Our work**
P2-type $K_{0.6}CoO_2$	1.7-4.0	100	120	38	60	2.7	216	3
P2-type $K_{0.6}CoO_2$	1.7-4.0	40	100 300	65 60	90 87	2.7	216	4
P3-type $K_{0.5}MnO_2$	1.5-3.9	20	50	70	70	2.6	260	5
$K_{0.5}V_2O_5$	1.5-3.8	100	250	48	81	2.6	280	6
P3-type $K_{0.69}CrO_2$	1.5-3.8	100	1000	52	65	2.3	230	7
P2-type $K_{0.65}Fe_{0.5}Mn_{0.5}O_2$	1.5-4.2	100	350	75	78	2.5	300	8
P3-type $K_{0.54}Co_{0.5}Mn_{0.5}O_2$	1.5-3.9	20 500	100 500	105 50	85 62	2.85	347	9
P2-type $K_{0.44}Ni_{0.22}Mn_{0.78}O_2$	1.5-4.0	200	500	58	67	2.5	362.5	10

References

1. X. Wang, K. Han, D. Qin, Q. Li, C. Wang, C. Niu and L. Mai, *Nanoscale*, 2017, **9**, 18216-18222.
2. Y. Wang, R. Xiao, Y. S. Hu, M. Avdeev and L. Chen, *Nat. Commun.*, 2015, **6**, 6954.
3. H. Kim, J. C. Kim, S.-H. Bo, T. Shi, D.-H. Kwon and G. Ceder, *Adv. Energy Mater.*, 2017, **7**, 1700098.
4. T. Deng, X. Fan, C. Luo, J. Chen, L. Chen, S. Hou, N. Eidson, X. Zhou and C. Wang, *Nano Lett.*, 2018, **18**, 1522-1529.
5. H. Kim, D. H. Seo, J. C. Kim, S. H. Bo, L. Liu, T. Shi and G. Ceder, *Adv. Mater.*, 2017, **29**, 1702480.
6. L. Deng, X. Niu, G. Ma, Z. Yang, L. Zeng, Y. Zhu and L. Guo, *Adv. Funct. Mater.*, 2018, **28**, 1800670.
7. J.-Y. Hwang, J. Kim, T.-Y. Yu, S.-T. Myung and Y.-K. Sun, *Energy Environ. Sci.*, 2018, **11**, 2821-2827.
8. T. Deng, X. Fan, J. Chen, L. Chen, C. Luo, X. Zhou, J. Yang, S. Zheng and C. Wang, *Adv. Funct. Mater.*, 2018, **28**, 1800219.
9. J. U. Choi, J. Kim, J.-Y. Hwang, J. H. Jo, Y.-K. Sun and S.-T. Myung, *Nano Energy*, 2019, **61**, 284-294.
10. X. Zhang, Y. Yang, X. Qu, Z. Wei, G. Sun, K. Zheng, H. Yu and F. Du, *Adv. Funct. Mater.*, 2019, **29**, 1905679.